

Discrimination of diverse coherences allows identification of electronic transitions of supermolecular nanoring

Vytautas Butkus,^{1, 2, a)} Jan Alster,^{3, b)} Eglė Bašinskaitė,^{1, 3} Ramūnas Augulis,^{3, 2}

Patrik Neuhaus,⁴ Leonas Valkunas,^{1, 2} Harry L. Anderson,⁴ Darius Abramavicius,¹ and Donatas Zigmantas^{3, c)}

¹⁾*Department of Theoretical Physics, Faculty of Physics, Vilnius University, Sauletekio Avenue 9-III, 10222 Vilnius, Lithuania*

²⁾*Center for Physical Sciences and Technology, Savanoriu Avenue 231, 02300 Vilnius, Lithuania*

³⁾*Department of Chemical Physics, Lund University, P.O. Box 124, SE-22100 Lund, Sweden*

⁴⁾*Department of Chemistry, University of Oxford, Chemistry Research Laboratory, Mansfield Road, Oxford OX1 3TA, United Kingdom*

The role of quantum coherence in photochemical functions of complex molecular systems such as photosynthetic units is a broadly debated topic. Coexistence and intermixing of electronic and/or vibrational coherences has been proposed to be responsible for the observed long-lived coherences. However, clear experimental characterization of coherences with different origin and their interconnection has been elusive. We present analysis of multidimensional spectra of a six-porphyrin nanoring supported by theoretical modeling that uncover a great diversity of separable electronic, vibrational and mixed coherences and show their cooperation in shaping the spectroscopic response. Results yield direct assignment of electronic and vibronic states and characterization of the excitation dynamics. Clear disentanglement of coherences in molecules with extended π -conjugation opens new avenues for exploring coherent phenomenon and understanding its importance for the function of the complex systems.

^{a)}These authors equally contributed to this work

^{b)}These authors equally contributed to this work ; Current address: Faculty of Mathematics and Physics, Charles University in Prague, Ke Karlovu 3, 121 16 Prague, Czech Republic

^{c)}Electronic mail: donatas.zigmantas@chemphys.lu.se

Versatile applications of organic polymers and other molecules with extended π -conjugation as electric charge carrying or light emitting/absorbing moieties allow facile and cheap production of optoelectronic devices¹. Even though they have been intensively studied, many questions remain due to their enormous chemical diversity, variability of optical and electronic properties, as well as due to the complex electronic structures of these materials.

Electronic energy transfer (EET) which is ubiquitous process in large supermolecular systems could be sensitive to coherent phenomena, arising from the quantum mechanical nature of the inner microscopic constituents. In the condition of electronic-vibrational resonance, quantum mixing of electronic and nuclear degrees of freedom of vibronically coupled molecular systems were suggested to result in a host of phenomena beyond the adiabatic approximation^{2,3}. Indeed, it has been shown that coupling to vibrational modes should enhance the rate of EET⁴⁻⁶ and of the charge transfer^{7,8}.

Coherences or evolving superposition of states in the form of quantum beats in large molecules has been observed for a long time⁹⁻¹¹. Recent developments of ultrafast nonlinear spectroscopic techniques, such as the two-dimensional electronic spectroscopy (2DES) facilitated more detailed investigations of coherences^{7,8,12-16}. However, even with simultaneously high spectral and temporal resolution provided by 2DES, the experimental identification of coherences and determination of their origin remains a highly complex issue. The nature of the long-lived coherences in the iconic Fenna-Matthews-Olson (FMO) light-harvesting complex (whether electronic¹⁷ or vibrational^{2,18,19}) is still hotly debated. Mechanisms related to electronic-vibrational mixing^{2,6,20}, inter-pigment correlations²¹ were proposed to be important, allowing FMO to maintain the quantum coherence for as long as a picosecond. Multiple aforementioned studies suggested coexistence of electronic and vibrational coherences in the same system and their interplay, however it has never been unambiguously discriminated.

To explore coherences of various origin we studied six-porphyrin nanoring complex. By analyzing two-dimensional beating maps we clearly identified three different types of coherences. This enabled us to determine the electronic origin of strongest optical absorption bands, which is quite unexpected for the system with a high degree of symmetry.

Results

The system. Nanoring, the structure of which is depicted in Fig. 1A and Fig S1, features multiple closely-spaced electronic and vibronic transitions and therefore is a well suited model system for gaining insight into electronic/vibronic transitions and variety of coherences. It consists of six zinc(II) porphyrin units forming a belt around an inner hexapyridyl template; the porphyrins contain aryl groups (3,5-bis(trihexylsilyl)benzene) at meso-positions and are interconnected by butadiyne links, ensuring complete π -conjugation of the nanoring. The fine structure of the main peaks identified as S_1 through S_6 in its absorption spectrum in methylcyclohexane solvent at 77 K (Fig. 1B) suggests that quantum superpositions of the states can be readily excited by short laser pulses and coherences should be clearly resolvable in 2DES measurements as oscillations.

Previous quantum chemistry calculations, using the time-dependent density functional theory, estimated the lowest-energy $S_0 - S_1$ transition at $\sim 10566 \text{ cm}^{-1}$. The sequence of similarly-spaced strong peaks (for the nanoring studied here found at 11655 cm^{-1} , 12295 cm^{-1} and 12862 cm^{-1}) was discussed in terms of the Franck-Condon progression of the vibrational mode or caused by dynamic vibronic coupling within a non-adiabatic framework²².

2D spectra of nanorings. We performed 2DES measurements on the hexamer nanorings at 77 K using laser pulses with spectrum centered either at 800 nm or 880 nm, thus covering different parts of the absorption (refer to the upper panels in Fig. 2A-B). The 2D spectrum at 30 fs waiting time, shown in Fig. 2A, was obtained with 880 nm laser pulses, which covered the lowest electronic transitions. The spectrum is dominated by a strong diagonal peak at $\sim 11655 \text{ cm}^{-1}$. Other features on the diagonal, related to the absorption, are observed at 10941 cm^{-1} (S_1) and 11373 cm^{-1} (S_2). These features are substantially weaker. However, the cross-peaks above the diagonal (P_{12} , P_{13} and P_{23}), correlating the three diagonal peaks can be clearly resolved. Excited state absorption shows up as negative features below the diagonal, masking positive cross-peaks.

Laser pulses with the spectrum centered at 800 nm were used to investigate the spectral range of the three most prominent transitions. The corresponding 2D spectrum at 30 fs waiting time is shown in Fig. 2B. The spectrum is abundant in features and at least 17 peaks can be resolved. Interestingly, a peak on the diagonal at around 11655 cm^{-1} consists of

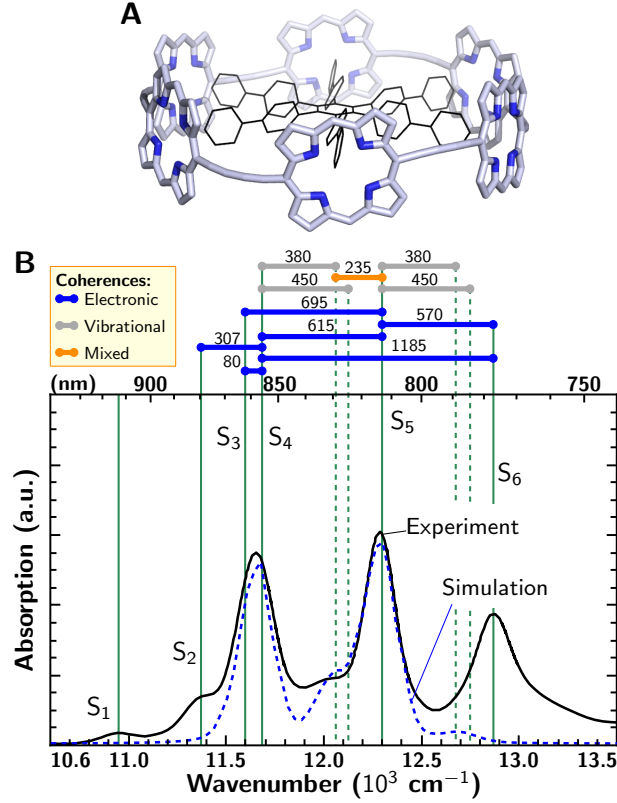


Figure 1. **Structure (A) and absorption spectrum (B) of the porphyrin nanoring.** (B) Measured (black solid line) and simulated by minimal vibronic model (blue dashed line) absorption spectra at 77 K. Energies of the electronic transitions to states $S_1 - S_6$ are indicated by vertical solid lines; vibronic transitions by vertical dashed lines. Frequencies of resolved coherent beatings are shown as colored segments, connecting the states involved in the corresponding quantum superpositions. The different colors signify the different origin of observed coherences.

two previously unresolved^{22,23} contributions separated by $\sim 80 \text{ cm}^{-1}$. It could be estimated from the position of the cross-peaks, indicated as P_{34} and P_{43} in Fig. 2C, that the energies corresponding to these states are approximately 11600 cm^{-1} (S_3) and 11680 cm^{-1} (S_4).

Coherent and incoherent dynamics. To measure coherent dynamics in the manifold of the excited states, 2DES data were acquired at a waiting time, t_2 , up to 800 fs, thus, making a complete 3D data set. Feature-rich oscillatory evolution was observed throughout the whole (ω_1, ω_3) 2D spectra as a function of t_2 . Another data set with waiting times up to 1 ns was measured to capture slower excitation relaxation processes. From the combined data, excitation population dynamics were extracted using a global fitting procedure with three exponential decays: a short time constant of 160 ± 250 fs and two longer lifetimes

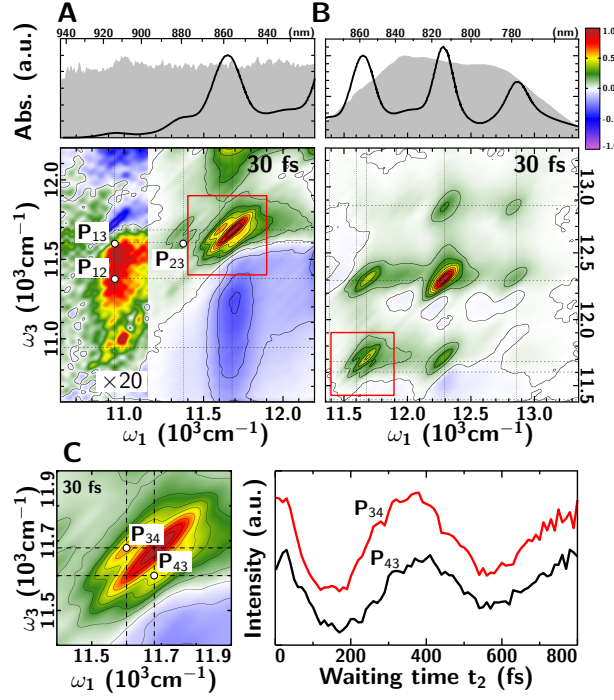


Figure 2. **Absorptive two-dimensional spectra at 30 fs waiting time.** Spectra were obtained using laser pulses centered at 880 nm (**A**) and 800 nm (**B**), respectively. In the upper panels nanoring absorption spectrum and laser intensity spectra are shown. In (**A**) the signal value is multiplied by a factor of 20 for the plot range where $\omega_1 < 11157 \text{ cm}^{-1}$. (**C**) Zoomed in region of a degenerate peak in the 800 nm measurement (shown by red squares in (**A**) and (**B**)) and oscillatory dynamics of the “P₃₄” and “P₄₃” peaks. Spectra are drawn using linear color scale, normalized to the maximum of each spectrum. Dashed vertical and horizontal lines indicate the energies of states $S_1 - S_6$.

of 235 ps and $\gg 1$ ns. The shortest timescale is related to downward energy relaxation in the singly-excited state manifold. This process is reflected in the decay of diagonal peaks in the 2D spectrum alongside the simultaneous increase of cross-peaks below the diagonal if no other competing channels exist^{24,25}. The longer timescales represent relaxation from the lowest state of the manifold to the ground or the other (for example, triplet) states (for more details see supplementary online materials text, Fig. S5 and S6).

Coherent beatings in the 2D spectra can be conveniently visualized by applying Fourier transforms $t_2 \rightarrow \omega_2$ to the residuals after subtraction of exponential decay components^{26,27}. The resulting Fourier amplitude dependency is a three-dimensional $(\omega_1, \omega_2, \omega_3)$ spectrum,

which can be analyzed by producing 2D slices (ω_1, ω_3) , so-called beating maps for a fixed frequency ω_2 . In the complex analysis of the oscillations evolution of Hermitian conjugate coherences $|a\rangle\langle b|$ and $|b\rangle\langle a|$ appear at positive and negative ω_2 frequencies, respectively^{27,28}.

The beating maps at a few selected ω_2 frequencies (see Fig. S2 for the full summary of observed coherences) are shown in Fig. 3A-D. Three types of peak configurations can be distinguished in measurements of nanorings. (i) The maps at $\omega_2 = \pm 80, \pm 307, \pm 570, \pm 615, \pm 695$, and $\pm 1150 \text{ cm}^{-1}$ shown in Fig. 3A-B are *diagonally symmetric*, i. e. positive and negative ω_2 features are mirror images of each other with respect to the diagonal as explicitly shown in Fig. 3A for $\omega_2 = \pm 80 \text{ cm}^{-1}$. (ii) Oscillation maps at $\omega_2 = +380 \text{ cm}^{-1}$ and -380 cm^{-1} , shown in Fig. 3C, are *diagonally asymmetric* and the features below the diagonal in the $\omega_2 = -380 \text{ cm}^{-1}$ map are significantly stronger than in the $\omega_2 = +380 \text{ cm}^{-1}$ map. (iii) Features in the $\omega_2 = -235 \text{ cm}^{-1}$ and $\omega_2 = +235 \text{ cm}^{-1}$ maps (Fig. 3D) are *diagonally asymmetric*, but their amplitudes are of similar magnitude for positive and negative frequency maps. Refer to Fig. S3 for extracted oscillation maps at the other distinguishable frequencies.

Discussion

Nature of coherences. It has been previously shown that electronic, vibrational, and mixed coherences are manifested by their characteristic patterns and symmetries in the beating maps^{3,29}. The symmetry of the experimental maps at $\omega_2 = \pm 80, \pm 307, \pm 570, \pm 615, \pm 695 \text{ cm}^{-1}$ and $\pm 1150 \text{ cm}^{-1}$ (Fig. 3A and B) indicate that the underlying coherences are of the electronic origin. Dephasing times of these coherences vary in the range of 80 - 500 fs, as determined by the time domain fitting procedure (Table I). These oscillations are present only on the off-diagonal regions in the rephasing 2D spectra (and only on the diagonal peaks in the non-rephasing 2D spectrum; see Fig. S4), and the peaks at positive and negative ω_2 frequencies in 2D slices are of the same amplitude.

The electronic coherence with $\omega_2 = +80 \text{ cm}^{-1}$ (and $\omega_2 = -80 \text{ cm}^{-1}$) can be assigned to the coherent superposition $|S_4\rangle\langle S_3|$ (and $|S_3\rangle\langle S_4|$) of the closely-positioned electronic states in the vicinity of 11655 cm^{-1} . The electronic coherence at $\omega_2 = \pm 307 \text{ cm}^{-1}$ shows up only in the measurement using laser pulses at 880 nm, signifying electronic quantum beats between states $|S_2\rangle$ and $|S_4\rangle$, that could not be excited by laser pulses at 800 nm. Beatings with

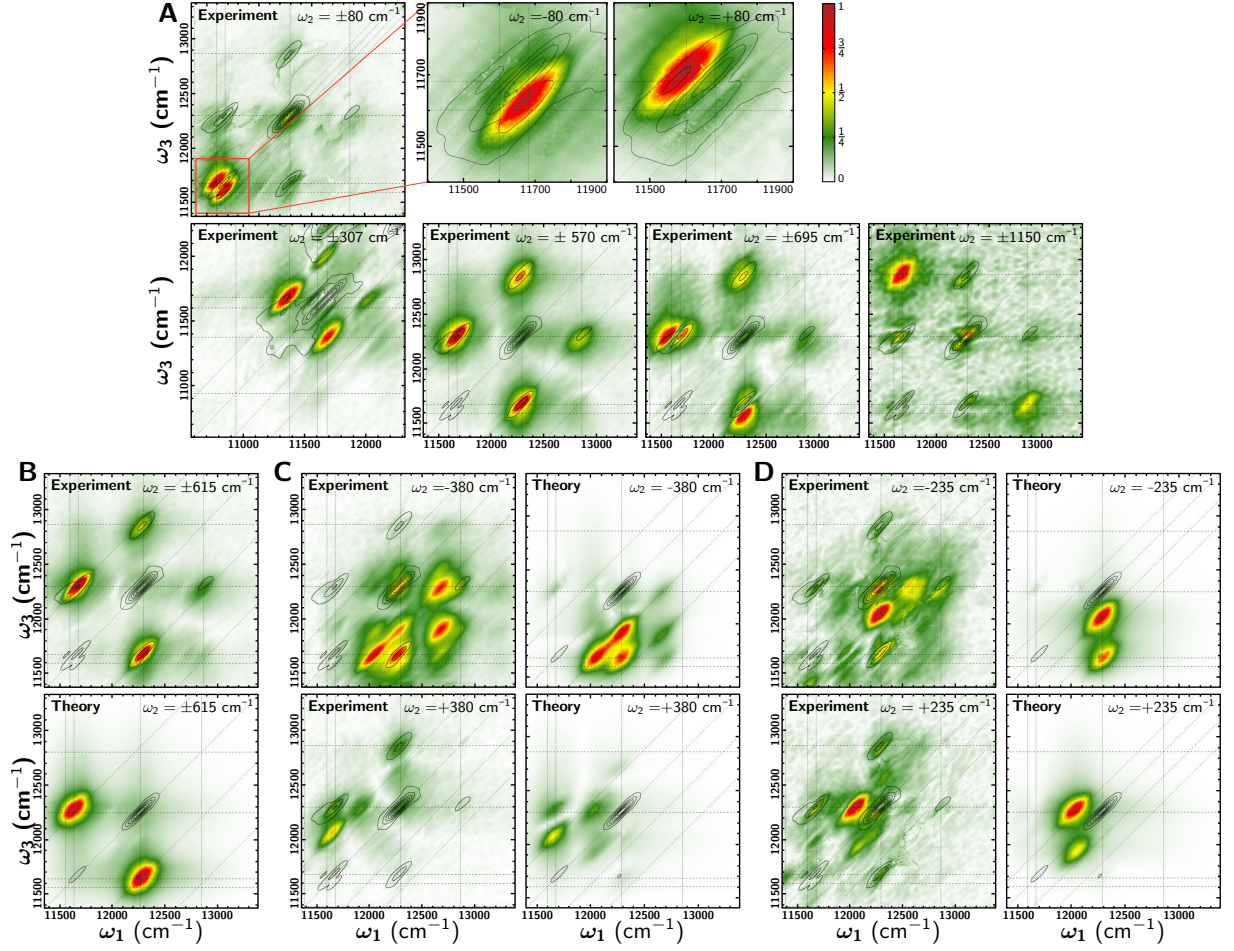


Figure 3. **Diversity of coherences revealed by oscillation maps.** (A) experimental beating maps of *electronic* coherences at $\omega_2 = \pm 80, \pm 307, \pm 570, \pm 695,$ and $\pm 1150 \text{ cm}^{-1}$; (B) experimental and simulated beating maps for the *electronic* coherence at $\omega_2 = \pm 615 \text{ cm}^{-1}$; (C) *the vibrational* coherence at $\omega_2 = \pm 380 \text{ cm}^{-1}$; (D) *the mixed* coherence at $\omega_2 = \pm 235 \text{ cm}^{-1}$. The oscillation amplitude at each point of a map is indicated by the color scale. Contours show 2D rephasing spectrum at 30 fs waiting time. Each experimental and theoretical map for a particular frequency is independently normalized to the maximum amplitude of the positive or negative frequency map. Dashed lines parallel to the diagonal are separated by the value of ω_2 . Dashed vertical and horizontal lines indicate transition frequencies of electronic states S_1 through S_6 . All, but $\omega_2 \pm 307 \text{ cm}^{-1}$ beating maps are extracted from the measurement with the laser spectrum at 800 nm. The $\omega_2 \pm 307 \text{ cm}^{-1}$ map was obtained from the 880 nm measurement.

Table I. **Classification of the observed coherences** ($<700 \text{ cm}^{-1}$). Average of four separate measurements are considered and the extracted dephasing times and standard deviations σ_τ are shown. The reliable dephasing times of a few coherences could not be extracted with a reliably defined experimental error. Dephasing times were obtained by fitting complex oscillatory signals in the time domain (for details, see the Supplementary Text online).

$\omega_2 \text{ (cm}^{-1}\text{)}$	Dephasing time (fs)	σ_τ (fs)	Origin of coherence
± 80	$\gtrsim 500$	~ 500	Electronic $ S_3\rangle\langle S_4 $
± 180	~ 500	~ 500	Vibrational
± 235	360	160	Mixed $ S_4^*\rangle\langle S_5 $
± 307	280	130	Electronic $ S_2\rangle\langle S_4 $
± 380	> 600	~ 500	Vibrational
± 450	~ 500	~ 500	Vibrational
± 570	80	20	Electronic $ S_5\rangle\langle S_6 $
± 615	200	30	Electronic $ S_4\rangle\langle S_5 $
± 695	190	40	Electronic $ S_3\rangle\langle S_5 $

the ± 570 , ± 615 , $\pm 695 \text{ cm}^{-1}$ and $\pm 1150 \text{ cm}^{-1}$ frequencies represent quantum coherences $|S_5\rangle\langle S_6|$, $|S_4\rangle\langle S_5|$, $|S_3\rangle\langle S_5|$ and $|S_4\rangle\langle S_6|$ (and their Hermitian conjugates). Multitude of purely electronic beatings provide evidence that the states $|S_2\rangle$ through $|S_6\rangle$ are of electronic origin in contrast to previous suggestions^{22,23}. Since $|S_2\rangle$ and $|S_3\rangle$ are the electronic states the clear correlation between $|S_1\rangle$ and $|S_2\rangle$, $|S_3\rangle$ states, as indicated by the cross-peaks in Fig. 2A, suggest that $|S_1\rangle$ is also an electronic state in accordance with the earlier studies²².

We find crosstalk in oscillation maps at $\omega_2 = \pm 570$, ± 615 , and $\pm 695 \text{ cm}^{-1}$ due to the overlap of different beating frequencies in the Fourier spectrum with limited resolution. For example, the appearance of two weaker peaks in the map of $\omega_2 = \pm 615 \text{ cm}^{-1}$ indicate the contribution from coherences $|S_4\rangle\langle S_5|$ with $\pm 570 \text{ cm}^{-1}$ frequency (Fig. 3B). The crosstalk between different frequencies is supported by the observation that in beating maps the weaker peaks are shifted away from the $\omega_3 = \omega_1 \pm 615 \text{ cm}^{-1}$ locations (dashed lines, parallel to the diagonal).

We assign beatings with the $\omega_2 = \pm 380 \text{ cm}^{-1}$ frequency to the vibrational coherence, which can be superposition of vibrational states in the ground and excited electronic state.

This follows from the oscillation maps (Fig. 3C), which have the pattern of oscillating signals typical for the vibrational coherence²⁹. The $\omega_2 = -380 \text{ cm}^{-1}$ map contains many features below the diagonal, while the $\omega_2 = +380 \text{ cm}^{-1}$ map is similar to the electronic beating maps presented in Fig. 3A and B. In contrast to the electronic coherences, the amplitude of the $\omega_2 = -380 \text{ cm}^{-1}$ map is significantly larger than that of $\omega_2 = +380 \text{ cm}^{-1}$ ^{12,30}. Detailed analysis of the maps implies that the vibrational ground state coherences $|g\rangle\langle g^*|$ ($|g^*\rangle$ denotes vibrationally hot ground state) appear exclusively at $\omega_2 < 0$ in rephasing maps. The large amplitude of peaks in negative frequency map is related to the long dephasing time of ground state vibrational superpositions, whereas vibrational superpositions on excited states mapped onto $\omega_2 = +380 \text{ cm}^{-1}$ dephase faster due to the energy relaxation in the excited states manifold. Maps at $\omega_2 = 128 \text{ cm}^{-1}$, 180 cm^{-1} and 450 cm^{-1} have much lower amplitude and assignment of corresponding frequencies is more difficult (see the supplementary online text), but judging by the pattern, the 450 cm^{-1} mode has vibrational origin.

Interestingly, beatings at $\omega_2 = \pm 235 \text{ cm}^{-1}$ clearly point out to the mixed character of the coherence, signifying the quantum superposition of the $|S_5\rangle$ electronic state and vibronically hot state $|S_4^*\rangle$ (with excited 380 cm^{-1} vibrational mode). The corresponding oscillation map is not similar to vibrational nor to electronic coherences (see Fig. 3D) and the beating frequency 235 cm^{-1} matches the energy gap between the identified states.

Simulation. To support the assignment of the excited states and the nature of the broad range of vibrational, electronic, and mixed coherences, the simple supermolecular vibronic model was considered. For qualitative simulations of the vibronic coupling in the supermolecular porphyrin nanoring we used the theoretical approach developed for a vibronic molecular dimer^{3,31}. Note that there have been several modeling studies published on exciton dynamics of porphyrin nanorings, see e.g.³². We assume that two electronic states with the highest oscillator strengths, S_4 and S_5 , are coupled to two vibrational modes with 380 cm^{-1} and 450 cm^{-1} frequencies with the Huang-Rhys factors of 0.03 and 0.01, respectively. The modeled absorption spectrum is presented in Fig. 1B by the dashed blue line. The model does not attempt to match absorption spectrum very well, instead our aim is to qualitatively reproduce the beating maps observed in the experiments. We performed simulations of the full 3D spectrum and extracted beating maps at various ω_2 values, corresponding to electronic, vibrational and mixed coherences (Fig. 3B, C and D). Although we included only two supermolecular excitonic states in the vibronic model, calculated and experimental

maps of the vibrational coherences at $\pm 380\text{ cm}^{-1}$, the electronic coherences at $\pm 615\text{ cm}^{-1}$, and the mixed coherences at $\pm 235\text{ cm}^{-1}$ are in a very good agreement with the experimental ones, confirming our assignments.

Summary and conclusions. Information on the strongest transitions and coherences in hexamer nanorings is summarized in Fig. 1B and Table I, respectively. The absorption spectrum of the porphyrin nanoring is dominated by electronic transitions. Energy from all higher-lying electronic and vibronic states relax to the the lowest S_1 state within 500 fs, which consequently decays to the ground state in a few hundred picoseconds. The wide range of observed dephasing times of electronic coherences (80-500 fs) suggests a varied degree of correlation between the electronic states. This implies differing extents of spatial delocalization of the electronic states in the nanoring, as it regulates dephasing times depending on the spatial overlap of the involved states. The observation that dephasing times of electronic coherences are in the same range as excitation energy relaxation, points to the possibility that coherently prepared electronic wavepackets may relax coherently through the manifold of electronic states in nanorings.

We observed and identified quantum coherences of all possible physical origins in a single supermolecule with extensive π -conjugation. We have demonstrated how analysis of coherences and their origin aids in disentangling the energy level structure of the excited states and provides a means to distinguish between electronic and vibronic features in spectroscopic signals. Due to the convoluted nature of electronic and vibrational degrees of freedom in molecular systems, the variety of coherences unraveled in this report should be present in any large molecule or molecular aggregate. The 2DES analysis of excitation dynamics presented here can be applied to any molecular system with a complex coupling network between electronic and vibrational transitions that dictates coherent and incoherent energy transfer dynamics.

ACKNOWLEDGMENTS

The work in Lund was supported by Swedish Research Council, the Knut and Alice Wallenberg Foundation, and the WennerÄSgren Foundation. The work in Oxford was supported by European Commission (Marie Curie Individual Fellowship to P. N. under contract PIEF-GA-2011-301336, the ERC), the EPSRC. V. B., E. B. and D. A. acknowledge the sup-

port of the Research Council of Lithuania (Grant No. MIP-090/2015). V.B. acknowledges support by project “Promotion of Student Scientific Activities” (VP1-3.1-MM-01-V-02-003) from the Research Council of Lithuania.

REFERENCES

- ¹H. S. Nalwa, ed., *Handbook of organic conductive molecules and polymers*, vol. 1–4 (John Wiley & Sons Chichester, 1997).
- ²V. Tiwari, W. K. Peters, D. M. Jonas, *Proc. Natl. Acad. Sci. USA* **110**, 1203 (2013).
- ³V. Butkus, L. Valkunas, D. Abramavicius, *J. Chem. Phys.* **140**, 034306 (2014).
- ⁴J. Womick, A. Moran, *J. Phys. Chem. B* **115**, 1347 (2011).
- ⁵A. Kolli, E. O’Reilly, G. Scholes, A. Olaya-Castro, *J. Chem. Phys.* **137**, 174109 (2012).
- ⁶A. W. Chin, *et al.*, *Nature Phys.* **9**, 113 (2013).
- ⁷F. D. Fuller, *et al.*, *Nature Chem.* **6**, 706 (2014).
- ⁸E. Romero, *et al.*, *Nat Phys* **10**, 676 (2014).
- ⁹M. H. Vos, F. Rappaport, J.-C. Lambry, J. Breton, J.-L. Martin, *Nature* **363**, 320 (1993).
- ¹⁰M. Chachisvilis, T. Pullerits, M. Jones, C. Hunter, V. Sundström, *Chem. Phys. Lett.* **224**, 345 (1994).
- ¹¹S. Savikhin, D. R. Buck, W. S. Struve, *Chem. Phys.* **223**, 303 (1997).
- ¹²G. Panitchayangkoon, *et al.*, *Proc. Natl. Acad. Sci. USA* **107**, 12766 (2010).
- ¹³A. Nemeth, *et al.*, *J. Chem. Phys.* **132**, 184514 (2010).
- ¹⁴S. Westenhoff, D. Paleček, P. Edlund, P. Smith, D. Zigmantas, *J. Am. Chem. Soc.* **134**, 16484 (2012).
- ¹⁵D. Hayes, G. B. Griffin, G. S. Engel, *Science* **340**, 1431 (2013).
- ¹⁶A. Halpin, *et al.*, *Nature Chem.* **6**, 196 (2014).
- ¹⁷G. Engel, *et al.*, *Nature* **446**, 782 (2007).
- ¹⁸N. Christensson, *et al.*, *J. Phys. Chem. B* **115**, 5383 (2011).
- ¹⁹R. Tempelaar, T. L. C. Jansen, J. Knoester, *The Journal of Physical Chemistry B* **118**, 12865 (2014).
- ²⁰N. Christensson, H. Kauffmann, T. Pullerits, T. Mančal, *J. Phys. Chem. B* **116**, 7449 (2012).
- ²¹D. Abramavicius, S. Mukamel, *J. Chem. Phys.* **134**, 174504 (2011).

- ²²J. K. Sprafke, *et al.*, *J. Am. Chem. Soc.* **133**, 17262 (2011).
- ²³M. Hoffmann, *et al.*, *Angew. Chem. Int. Ed.* **47**, 4993 (2008).
- ²⁴T. Brixner, *et al.*, *Nature* **434**, 625 (2005).
- ²⁵J. Dostál, F. Vácha, J. Pšenčík, D. Zigmantas, *J. Phys. Chem. Lett.* **5**, 1743 (2014).
- ²⁶N. Christensson, *et al.*, *J. Phys. Chem. B* **117**, 11209 (2013).
- ²⁷H. Li, A. D. Bristow, M. E. Siemens, G. Moody, S. T. Cundiff, *Nat. Commun.* **4**, 1390 (2013).
- ²⁸J. Seibt, T. Hansen, T. Pullerits, *J. Phys. Chem. B* **117**, 11124 (2013).
- ²⁹V. Butkus, D. Zigmantas, L. Valkunas, D. Abramavicius, *Chem. Phys. Lett.* **545**, 40 (2012).
- ³⁰V. Butkus, D. Zigmantas, D. Abramavicius, L. Valkunas, *Chem. Phys. Lett.* **587**, 93 (2013).
- ³¹E. Bašinskaitė, V. Butkus, D. Abramavicius, L. Valkunas, *Photosynth. Res.* **121**, 95 (2014).
- ³²P. Parkinson, *et al.*, *The Journal of Physical Chemistry Letters* **5**, 4356 (2014).